Adaptive fuzzy hysteresis internal model tracking control of piezoelectric actuators with nanoscale application

Pengzhi Li, Peiyue Li and Yongxin Sui

***Abstract*—In this paper, a novel Takagi-Sugeno (T-S) fuzzy-system-based model is proposed for hysteresis in piezoelectric actuators. The antecedent and consequent structures of the developed fuzzy hysteresis model (FHM) can be identified on-line through uniform partition approach and recursive least squares (RLS) algorithm respectively. With respect to the controller design, the inverse of FHM is used to develop a fuzzy internal model (FIM) controller. Decreasing the hysteresis effect, the FIM controller has a good performance of high-speed trajectory tracking. To achieve nanometer-scale tracking precision, the novel fuzzy adaptive internal model (FAIM) controller is uniquely developed. Based on real-time input and output data to update FHM, the FAIM controller is capable of compensating for the hysteresis effect of the piezoelectric actuator in real time. Finally, the experimental results for two cases are shown, the first is with 50 Hz and the other with multiple frequency (50Hz+25Hz) sinusoidal trajectories tracking that demonstrate the efficiency of the proposed controllers. Especially, being 0.32% of the maximum desired displacement, the maximum error of 50 Hz sinusoidal tracking is greatly reduced to 6 nm. This result clearly indicates the nanometer-scale tracking performance of the novel FAIM controller.**

***Index Terms*—fuzzy adaptive internal model, T-S, trajectory tracking, hysteresis, piezoelectric actuator**

I. Introduction

THE lead-zirconate-titanate piezoelectric ceramics (PZT) in use today are mainly $PbTiO_3$-$PbZrO_3$ compounds. The piezoelectric actuator (also referred as PZT) is mainly composed of piezoelectric ceramics. Because of its high bandwidth, nanometer displacement resolution and zero mechanical friction, the piezoelectric actuator is widely used in micro-/nano-manipulation [1], micro-/nano-positioning [2], [3], [4] and optics [5], [6]. However, the intrinsic nonlinear and multi-valued hysteresis in the piezoelectric actuator has the potential to cause inaccuracy or even instability of its applied system. The maximum error resulting from the hysteresis can be as much as 10%-15% of the path covered [7].

The hysteresis is often characterized by nonlinearity and rate-dependence. Nonlinearity means that the same input voltage results in different output displacements during the course of voltage increase and decrease. There is no one-to-one relationship between voltage and displacement. Besides, rate-dependence indicates that the frequency of input voltage has influence on the shape and orientation of hysteresis curve.

In the last decade, many models such as Preisach model [8], [9], Prandtl-Ishlinskii (PI) model [10], Maxwell slip model [11], Duhem model [12], [13] and Jiles-Atherton model [14] have been presented mainly for rate-independent hysteresis. For rate-dependent hysteresis, Refs. [15], [16] and [17] proposed several modified PI models combining neural network or a density function of time rate of input. Recently, autoregressive moving average (ARMA)-based [18] model and automatic real-time vision-based [19] method were developed for hysteresis in piezoelectric actuators. Feedforward controller, feedback controller and complex controller with both feedforward and feedback schemes have also been developed for hysteresis compensation in the piezoelectric actuator. Ref. [20] showed that iterative inversion-based feedforward control could be used to compensate for the dynamics-coupling error in piezoscanners during high-speed positioning. Sliding mode control strategies [21], [22], [23] were adopted for trajectory tracking of the piezoelectric actuator. Ref. [24] proposed a closed-loop rate-independent hysteresis compensator for a stacked PZT actuator from a congruency-based hysteresis model. Support vector machine model-based complex controller [25] was designed to suppress the rate-dependent hysteresis.

Among many control schemes, internal model control has displayed a conspicuous popularity in process control industry due to its good robustness against disturbances and model mismatch [26], [27]. The basic structure of an internal model control scheme is usually composed of the internal model controller, the plant, the plant model and the feedback filter. In fact, the determination of the plant model plays an important role in the development of internal model control. The internal model controller can be directly obtained via the inversion of the plant model. The feedback filter is generally designed to alleviate sensitivity problems. If the plant model matches the plant exactly, a perfect disturbance rejection and trajectory tracking will be achieved. Thus, the major task of an internal model control scheme is to find a precise plant model.

Recently, fuzzy system has been broadly utilized in nonlinear modelling [28], [29], [30], [31] and automatic control [32], [33], [34], [35]. This paper proposes a simple Takagi-Sugeno (T-S) [36], [37] fuzzy-system-based model for both rate-independent and rate-dependent hysteresis. The fuzzy hysteresis model (FHM) uses uniform partition approach and

Manuscript received xx. This work is supported by the National Key Scientific and Technological Special Project of China under Grant 2009ZX02205.

Pengzhi Li, Peiyue Li and Yongxin Sui are with the Engineering Research Center of Extreme Precision Optics, State Key Laboratory of Applied Optics, Changchun Institute of Optics, Fine Mechanics and Physics, Chinese Academy of Sciences, Changchun 130033, China (e-mail: kindrobot@163.com; lipy@sklao.ac.cn; suiyx@sklao.ac.cn).

recursive least squares (RLS) algorithm for identification and optimization. The inverse of FHM is used to design a fuzzy internal model (FIM) controller to decrease the hysteresis effect. To achieve nanometer-scale tracking precision, the novel fuzzy adaptive internal model (FAIM) controller is uniquely developed. For two cases of periodic trajectories tracking, experimental results demonstrate the efficiency of the proposed controllers.

The organization of this paper is as follows. Section I gives a brief introduction. In Section II, the structure, identification and inverse of FHM is proposed. Section III presents the developed controllers. Section IV includes the experimental setup and results. In Section V, a summary of the paper is given.

II. Fuzzy hysteresis model

Generally, a fuzzy system is composed of a fuzzifier, fuzzy rule base, fuzzy inference engine and defuzzifier. The fuzzifier transforms real-valued input variables to fuzzy sets. The fuzzy rule base can be viewed as sets of many fuzzy IF-THEN rules. The fuzzy inference engine adopts individual-rule or composition based inference method to map fuzzy sets in the input universe of discourse $U \subset R^n$ to ones in the output universe of discourse $Y \subset R$ based on some fuzzy logic. The defuzzifier transforms fuzzy sets in $Y \subset R$ to real-valued output. Especially, without the fuzzifier and defuzzifier, T-S fuzzy system has real-valued input and output variables. Appropriate for modelling nonlinear systems, it is chosen to model hysteresis in the piezoelectric actuator.

A. FHM structure

A discrete-time PZT system with hysteresis is considered. The T-S FHM has the following fuzzy rules:

$$\begin{aligned} R^l\text{: IF } & y(k-1) \text{ is } A^l, \\ \text{THEN } & y(k) = q_{l1}y(k-1) + q_{l2}u(k) + q_{l3}, \end{aligned} \tag{1}$$

where $y(k) = y(kT_\mathrm{s}) = y_k, u(k) = u(kT_\mathrm{s}) = u_k$ are the output and input of PZT system at the time instant kT_s respectively, T_s is the sampling period, q_{l1}, q_{l2}, q_{l3} are real-valued parameters of the consequent part (i.e. THEN part of the fuzzy rule), $l = 1, \cdots, L$, L is the number of fuzzy rules.

A^l is a fuzzy set with triangular membership function $\mu_{A^l}(y_{k-1})$ defined as

$$\mu_{A^l}(y_{k-1}) = \begin{cases} 1 - |y_{k-1} - c_l|/a_l, & y_{k-1} \in [c_l - a_l, c_l + a_l] \\ 0, & otherwise \end{cases} \tag{2}$$

where c_l, a_l are the parameters of the membership function in the premise part (i.e. IF part of the fuzzy rule). Compared with the Gaussian exponential membership function, the advantage of the triangular membership function lies in little computational burden without the loss of modelling accuracy.

The fuzzy basis function (FBF), which can also be referred as weighted firing strength, is given by

$$p^l(y_{k-1}) = \frac{\mu_{A^l}(y_{k-1})}{\sum_{l=1}^{L}\left(\mu_{A^l}\left(y_{k-1}\right)\right)}. \tag{3}$$

Finally, the weighted average output $\hat{y}_k$ of FHM is

$$\hat{y}_k = \sum_{l=1}^{L}\left(p^l(y_{k-1})\left(q_{l1}y(k-1) + q_{l2}u(k) + q_{l3}\right)\right). \tag{4}$$

It should be noted that fuzzy rule of Eq. (1) is actually equivalent to the following one:
R^l: IF $y(k-1)$ is A^l and $u(k)$ is I^l,
THEN $y(k) = q_{l1}y(k-1) + q_{l2}u(k) + q_{l3},\ l = 1, \cdots, L$,
where I^l is a fuzzy set with the membership function $\mu_{I^l}(u_k) = 1$. The advantages are as follows:

- FHM identification of premise parameters is simplified without considering u_k.
- The analytic inverse of FHM is easily obtained without u_k in the premise part of fuzzy rule.

B. FHM identification

In order to solve the hysteresis problem of multi-valued mapping, herein extended input variable is used. Suppose N pairs of experimental data $(y_k, u_k) = (y(k), u(k)), k = 1, \cdots, N$ have been sampled. The premise parameters c_l, a_l and consequent parameters $q_{l1}, q_{l2}, q_{l3}, l = 1, \cdots, L$ need to be identified for FHM.

For premise parameters $c_l, a_l, l = 1, \cdots, L$, due to the specially designed 'partial' fuzzy rule, the input variable y_{k-1} is partitioned uniformly. Suppose numerical range of $y_{k-1}, k = 1, \cdots, N$ is $[y_{\min}, y_{\max}]$, then

$$c_l = y_{\min} + (y_{\max} - y_{\min})(l-1)/(L-1), \tag{5}$$

$$a_1 = a_2 = \cdots = a_L = (y_{\max} - y_{\min})/(L-1). \tag{6}$$

Herein the premise part of FHM has been obtained; that is to say, fuzzy sets $A^l, l = 1, \cdots, L$ have been known, illustrated as Fig. 1. The fuzzy sets are normal, complete and consistent. This uniform partition method is computationally easier than both subtractive clustering and fuzzy C-means clustering algorithms. Besides, it can be applied on-line.

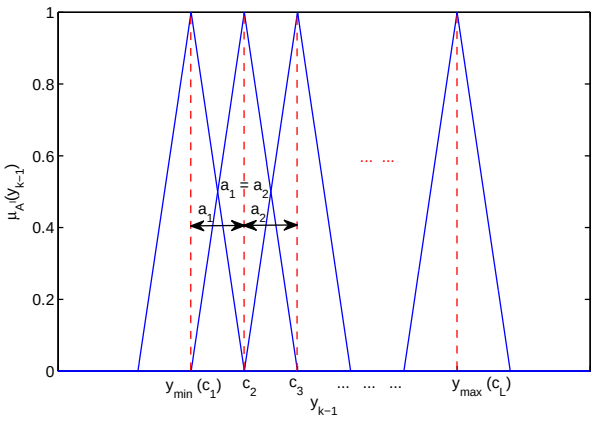

Fig. 1. Uniform partition of y_{k-1} in the premise part of FHM.

Next, the consequent parameters $q_{l1}, q_{l2}, q_{l3}, l = 1, \cdots, L$ are optimized by using RLS algorithm. The performance criterion is chosen as:

$$J = \frac{1}{2}\sum_{k=1}^{N}\left(e_\mathrm{m}(k)\right)^2 = \frac{1}{2}\sum_{k=1}^{N}\left(y(k) - \hat{y}_k\right)^2. \tag{7}$$

The vectors for the consequent parameters and extended input can be defined as

$$\begin{aligned}
&\boldsymbol{q}_l = [q_{l1}, q_{l2}, q_{l3}]^T, \boldsymbol{q}_l \in R^{3\times 1},\\
&\tilde{\boldsymbol{u}}_k = [y_{k-1}, u_k, 1]^T, \tilde{\boldsymbol{u}}_k \in R^{3\times 1},\\
&\boldsymbol{q} = \left[\boldsymbol{q}_1^T, \boldsymbol{q}_2^T, \cdots, \boldsymbol{q}_L^T,\right]^T, \boldsymbol{q} \in R^{(3L)\times 1},\\
&\bar{\boldsymbol{u}}_k = \left[p^1(y_{k-1})\tilde{\boldsymbol{u}}_k^T, p^2(y_{k-1})\tilde{\boldsymbol{u}}_k^T, \cdots, p^L(y_{k-1})\tilde{\boldsymbol{u}}_k^T\right]^T,\\
&\quad \bar{\boldsymbol{u}}_k \in R^{(3L)\times 1}.
\end{aligned} \tag{8}$$

Then $\hat{y}_k$ of Eq. (4) can be rewritten as:

$$\begin{aligned}
\hat{y}_k &= \sum_{l=1}^{L}\left(p^l(y_{k-1})\left(\boldsymbol{q}_l^T\cdot\tilde{\boldsymbol{u}}_k\right)\right)\\
&= p^1(y_{k-1})\tilde{\boldsymbol{u}}_k^T\cdot\boldsymbol{q}_1 + p^2(y_{k-1})\tilde{\boldsymbol{u}}_k^T\cdot\boldsymbol{q}_2 + \cdots\\
&\quad + p^L(y_{k-1})\tilde{\boldsymbol{u}}_k^T\cdot\boldsymbol{q}_L\\
&= \bar{\boldsymbol{u}}_k^T\cdot\boldsymbol{q}.
\end{aligned} \tag{9}$$

Then RLS algorithm at each time instant $k = 1, 2, \cdots, N$ can be written as:

$$\begin{aligned}
\boldsymbol{q}(k) &= \boldsymbol{q}(k-1) + \mathbf{P}(k-1)\bar{\boldsymbol{u}}_k\frac{y(k) - \bar{\boldsymbol{u}}_k^T\cdot\boldsymbol{q}(k-1)}{\lambda + \bar{\boldsymbol{u}}_k^T\mathbf{P}(k-1)\bar{\boldsymbol{u}}_k},\\
\mathbf{P}(k) &= \left(\mathbf{I} - \frac{\mathbf{P}(k-1)\bar{\boldsymbol{u}}_k\bar{\boldsymbol{u}}_k^T}{\lambda + \bar{\boldsymbol{u}}_k^T\mathbf{P}(k-1)\bar{\boldsymbol{u}}_k}\right)\frac{\mathbf{P}(k-1)}{\lambda},
\end{aligned} \tag{10}$$

where $\mathbf{P} \in R^{(3L)\times(3L)}, \mathbf{I} \in R^{(3L)\times(3L)}$ is an identity matrix and $\lambda \in (0, 1]$ is the forgetting factor. The initial parameters can be chosen as $\mathbf{P}(0) = \alpha\mathbf{I}$ and $\boldsymbol{q}(0) = \varepsilon\left[1, 1, \ldots\right]^T$ respectively. α is a big positive constant value and ε is a small positive constant or zero value. The RLS algorithm can be easily applied on-line. In the following paragraph, parameters are selected as $\lambda = 1, \alpha = 1\times 10^6$ and $\varepsilon = 0$.

C. FHM inverse

After the premise parameters c_l, a_l and consequent parameters $q_{l1}, q_{l2}, q_{l3}, l = 1, \cdots, L$ have been identified, from Eq. (4) the inverse u_{inv} of FHM can be analytically obtained.

Rewrite Eq. (4) as

$$\hat{y}_k\left(\sum_{l=1}^{L}\left(\mu_{A^l}\left(y_{k-1}\right)\right)\right) =$$

$$\sum_{l=1}^{L}\left(\mu_{A^l}(y_{k-1})\left(q_{l1}y(k-1) + q_{l2}u(k) + q_{l3}\right)\right) =$$

$$u(k)\sum_{l=1}^{L}\left(\mu_{A^l}(y_{k-1})q_{l2}\right) + \sum_{l=1}^{L}\left(\mu_{A^l}(y_{k-1})\left(q_{l1}y(k-1) + q_{l3}\right)\right),$$

then transpose it as

$$u(k)\sum_{l=1}^{L}\left(\mu_{A^l}(y_{k-1})q_{l2}\right) =$$

$$\hat{y}_k\left(\sum_{l=1}^{L}\left(\mu_{A^l}\left(y_{k-1}\right)\right)\right) - \sum_{l=1}^{L}\left(\mu_{A^l}(y_{k-1})\left(q_{l1}y(k-1) + q_{l3}\right)\right),$$

finally, by substituting $u_{\text{inv}}(k)$ for $u(k)$ and $y(k)$ for $\hat{y}_k$, the inverse of FHM can be attained as

$$u_{\text{inv}}(k) = \frac{y(k)\left(\sum_{l=1}^{L}\left(\mu_{A^l}\left(y_{k-1}\right)\right)\right) - \sum_{l=1}^{L}\left(\mu_{A^l}(y_{k-1})\left(q_{l1}y(k-1) + q_{l3}\right)\right)}{\sum_{l=1}^{L}\left(\mu_{A^l}(y_{k-1})q_{l2}\right)}. \tag{11}$$

It implies that an inverse-model-based internal model controller can be designed to compensate for the nonlinear hysteresis effect of PZT system.

D. FHM computational time complexity

With regard to the modern digital signal processor (DSP), the computational time complexity [38] in this paper is approximately defined as how many multiplication and division operations performed during each sampling period by FHM. Denote $T(i)$ as the computational time complexity of the ith equation, then

$$\begin{aligned}
T(2) &= 1,\\
T(4) &= 6L + 1 = O(L),\\
T(10) &= (3L)^3 + 4(3L)^2 + 5(3L) + 2\\
&= 27L^3 + 36L^2 + 15L + 2 = O(L^3),\\
T(11) &= 7L + 2 = O(L).
\end{aligned} \tag{12}$$

More details of the computational time complexity about the proposed controllers and its applications in the practical controller implementation will be given in Section III and Section IV.

III. Tracking controller design

Fig. 2 shows the block diagram of the controller implementation. The module Z^{-1} represents one sampling period delay. The module *Fuzzy Internal Hysteresis Model* serves as the function of plant model, working according to Eq. (4). The module *Inverse Fuzzy Internal Model Controller* serves as the function of internal model controller, running according to Eq. (11). The module *Feedback Filter* is actually a low-pass filter and very important to the robustness of the overall controller. The module *Fuzzy Adaptive Hysteresis Model* uses real-time input and output of PZT stage to make FHM adapted to on-site hysteresis characteristics according to Eqs. (5), (6) and (10).

In practical applications, FHM is never perfect, resulting in a non-null error of model mismatch. The error may deteriorate performance or even cause instability of the overall controller. Hence, a filter is often added for robustness. With unit gain, the module *Feedback Filter* has the following discrete-time transfer function

$$\frac{1-\beta}{1-\beta z^{-1}} = \frac{(1-\beta)z}{z-\beta}. \tag{13}$$

Generally, for closed-loop stability of the overall controller, the parameter β of the filter is chosen as $\beta \in (0, 1)$.

For comparison, the conventional PID controller is also employed. It is widely used in industrial processes due to

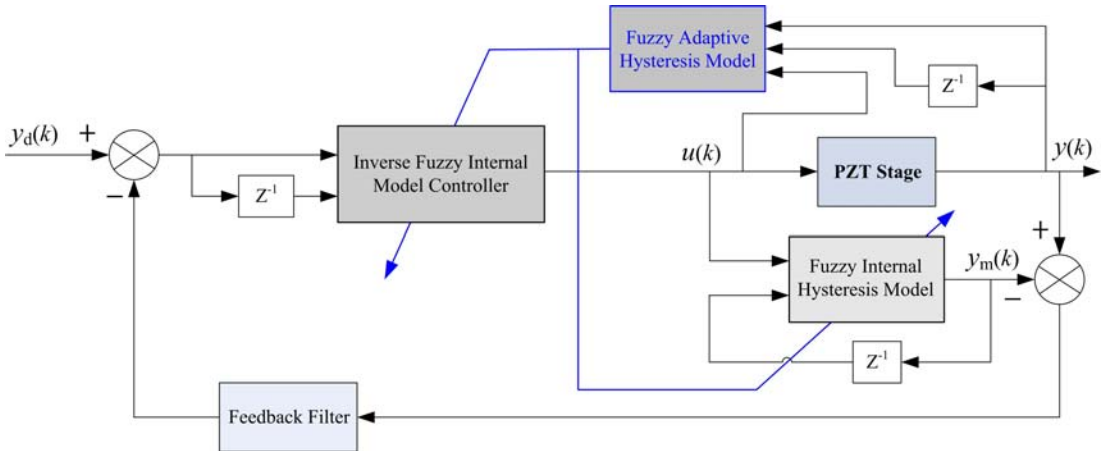

Fig. 2. Block diagram of the overall controller.

its simplicity, applicability and ease of use [39]. Here, the discrete-time incremental PID algorithm is adopted as follows:

$$\begin{aligned} u(k) &= u(k-1) + \Delta u(k), \\ \Delta u(k) &= k_{\mathrm{p}}\left(e(k) - e(k-1)\right) + k_{\mathrm{i}} e(k) \\ &\quad + k_{\mathrm{d}}\left(e(k) - 2e(k-1) + e(k-2)\right), \end{aligned} \tag{14}$$

where $k_{\mathrm{p}}, k_{\mathrm{i}}$ and k_{d} are the proportional gain, integral gain and derivative gain respectively. It is often a process of trial and error to find suitable or even optimum PID parameters.

A. Fuzzy internal model controller

Without the module *Fuzzy Adaptive Hysteresis Model* working, the overall controller is equivalent to a fuzzy internal model controller. First, based on collected input and output data of PZT system, a suitable FHM is obtained off-line in advance. Then, using the obtained FHM and its inverse, the modules *Fuzzy Internal Hysteresis Model* and *Inverse Fuzzy Internal Model Controller* work, and the FIM controller tracks the desired trajectory y_{d}. Its tracking performance is mainly concerned with the generality and match precision of the obtained FHM. The computational time complexity of the FIM controller is $T_{\mathrm{FIM}} = T(4) + T(11) = 13L + 3 = O(L)$.

B. Fuzzy adaptive internal model controller

With the module *Fuzzy Adaptive Hysteresis Model* working, the overall controller acts as a fuzzy adaptive internal model controller. It can achieve better tracking performance than FIM controller due to the real-time updating of FHM. The working procedure of FAIM controller is as follows.

1) Use initial FHM identified off-line to run the FIM controller for i periods of y_{d}.
2) Treat y_{d} as the input variable, and then uniformly partition y_{d} according to Eqs. (5) and (6) to obtain the premise parameters of future adaptive FHM.
3) During ith period, according to Eq. (10), use real-time input and output data of PZT system to update the consequent parameters at each time instant. After the ith period ends, notated as FHM_i, the adaptive FHM of ith period is obtained.
4) During the next period, i.e. $(i+1)$th period, use FHM_i to run the FAIM controller. Meanwhile, increase i by 1, execute 3) in parallel.
5) Return to 4) for the next period.

The following are some remarks about the design of FAIM controller.

- The premise parameters of adaptive FHM are updated according to y_{d}, not real-time output y of PZT system. First, y_{d} are known in advance, so this process needs to be updated just once. It can greatly reduce the real-time computational burden. Second, the control objective is to make y track y_{d}, so it is reasonable to replace y with y_{d}.
- As y_{d} are commonly periodic, the updating process, i.e. working of the module *Fuzzy Adaptive Hysteresis Model*, is executed every period of y_{d}. The data of only one period are used to update the FHM. That is to say, during $(i+1)$th period, the working modules *Fuzzy Internal Hysteresis Model* and *Inverse Fuzzy Internal Model Controller* are based on the updated FHM_i, and the updating FHM_{i+1} of current period is intended to change the FAIM controller of next period. First, for more general implementation, initial FHM and FIM controller are not always optimum. Second, the updating of current FHM works in parallel with current FAIM controller and only affects it during next period. It can avert unnecessary oscillations and moreover reduce the real-time computational burden.
- The computational time complexity of the FAIM controller is $T_{\mathrm{FAIM}} = T_{\mathrm{FIM}} + T(10) = 27L^3 + 36L^2 + 28L + 5 = O(L^3)$, which is considerably demanding. Its application in the practical implementation of FAIM controller will be discussed in Section IV.

C. Stability of the controller

According to Eq. (4), the output $y(k)$ of PZT stage in Fig. 2 can be represented as

$$\begin{aligned} y(k) &= \frac{\sum_{l=1}^{L}\left(\mu_{A^l}(y_{k-1})\left(q_{l1}y(k-1)+q_{l3}\right)\right)}{\sum_{l=1}^{L}\left(\mu_{A^l}\left(y_{k-1}\right)\right)} \\ &\quad + \frac{\sum_{l=1}^{L}\left(\mu_{A^l}(y_{k-1})q_{l2}\right)}{\sum_{l=1}^{L}\left(\mu_{A^l}\left(y_{k-1}\right)\right)}u(k) + \xi(k) + d(k) \\ &= f(y(k-1)) + g(y(k-1))u(k) + \xi(k) + d(k) \\ &= f(k-1) + g(k-1)u(k) + \xi(k) + d(k), \end{aligned} \tag{15}$$

where $\xi(k)$ is the modelling error of FHM, $d(k)$ is the noise and disturbance, $f(\cdot)$ and $g(\cdot)$ are nonlinear functions of $y(k-1)$ respectively.

Assumption 1: The PZT stage is stable in the open loop, the stable inverse of FHM exists and $g \neq 0$.

Assumption 2: $|\xi(k)| \leq \xi_0$, $|d(k)| \leq d_0$, ξ_0 and d_0 are positive values, and $\bar{\xi} = \xi_0 + d_0$.

Based on Assumption 1, the control law $u(k)$ in Fig. 2 can be expressed as

$$u(k) = g^{-1}(k-1)\left(y_d(k) - f(k-1) - F(z)(\xi(k)+d(k))\right), \tag{16}$$

where $F(z)$ is the representation of the module *Feedback Filter*.

Define $e(k) = y_d(k) - y(k)$, then

$$\begin{aligned} e(k+1) &= y_d(k+1) - y(k+1) \\ &= y_d(k+1) - (f(k) + \xi(k+1) + d(k+1) \\ &\quad + g(k)u(k+1)). \end{aligned} \tag{17}$$

According to Eq. (16), Eq. (17) can be rewritten as

$$\begin{aligned} e(k+1) &= y_d(k+1) - (f(k) + \xi(k+1) + d(k+1) \\ &\quad + g(k)g^{-1}(k)(y_d(k+1) - f(k) \\ &\quad - F(z)(\xi(k+1) + d(k+1)))) \\ &= -(1 - F(z))(\xi(k+1) + d(k+1)). \end{aligned} \tag{18}$$

Define the Lyapunov function candidate $V(k) = e^2(k)$, and

$$\begin{aligned} &V(k+1) - V(k) \\ &\quad = e^2(k+1) - e^2(k) \\ &\quad = \left((1 - F(z))(\xi(k+1) + d(k+1))\right)^2 - e^2(k) \\ &\quad \leq (1 - F(z))^2(|\xi(k+1)| + |d(k+1)|)^2 - e^2(k) \\ &\quad \leq (1 - F(z))^2(\xi_0 + d_0)^2 - e^2(k) \\ &\quad = (1 - F(z))^2\bar{\xi}^2 - e^2(k). \end{aligned} \tag{19}$$

When $|e(k)| > |1 - F(z)|\bar{\xi}$, $V(k+1) - V(k) < 0$, so the tracking error $e(k)$ is bounded by $\lim_{k\to\infty}|e(k)| \leq |1 - F(z)|\bar{\xi}$.

In fact, because the main focus of the paper is the application of the piezoelectric actuator in nanometer-scale ultra-precise tracking, the noise and disturbance is greatly diminished by fixing the experiment equipment on a vibration isolation mounting in a laboratory under precise environmental control. Besides, the modelling error can be progressively minimized via the updating of adaptive FHM. Hence suitable filter can be chosen for both stability and excellent performance of the designed controllers in the practical tracking experiments.

IV. Experimental results

As shown in Fig. 3, a nano-positioning stage driven by piezoelectric actuators (PICMA P-885.30) is built as the experimental platform. The piezoelectric actuator has a nominal displacement of 0-10 μm and an operating voltage range from -20 to 120 V. Other experimental equipment includes a digital controller and built-in capacitive sensors (D-015.00). The digital controller consists of a floating-point DSP, a voltage amplifier (E-503.00) with 10$\times$ gain, a signal conditioner (E-509.C3A) for capacitive sensors, 16 bits A/D and 20 bits D/A converters. The floating-point DSP specially conducts the tracking control. The capacitive sensors have a displacement resolution less than 0.5 nm. The equipment mentioned above is mainly provided by Physik Instrumente GmbH & Co. KG in Germany. The experiment is carried out in a laboratory under precise environmental control, and the ambient temperature of the laboratory is kept at 22$\pm$0.5 degree Celsius. All the equipment is fixed on a vibration isolation mounting. The experimental sampling frequency is selected as 1 kHz, which means the sampling period T_s is 1 ms. The diagram of the experimental layout is illustrated in Fig. 4.

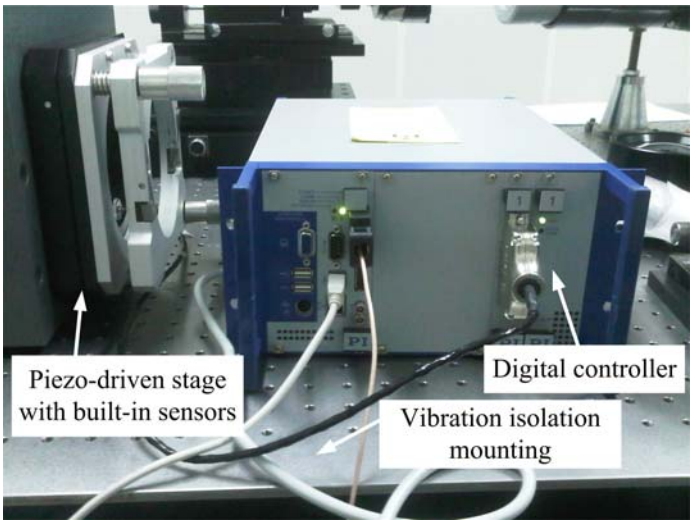

Fig. 3. Experimental platform driven by the piezoelectric actuator: the capacitive sensors are built in the piezo-driven stage; the floating-point DSP, voltage amplifier, signal conditioner, A/D and D/A converters are all located in the digital controller.

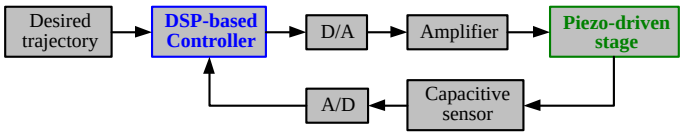

Fig. 4. The diagram of the experimental layout: the real-time displacement of the piezo-driven stage is measured by the capacitive sensor; with the input of the displacement and desired trajectory, the DSP-based controller implements the proposed FIM and FAIM control strategy; the output of the controller is amplified by the amplifier and then excites the piezo-driven stage.

In tracking control applications of piezoelectric actuators, periodic waveforms are commonly used as desired trajectories. Two cases of waveforms are chosen as y_d: single frequency sinusoidal and multiple frequency sinusoidal waveforms. Single

frequency sinusoidal waveforms are widely used as a result of continuous differentiability. Multiple frequency sinusoidal waveforms can exhibit rate-dependent hysteresis characteristics. These cases can comprehensively check the effectiveness of the designed controllers.

Three different controllers are used in our experiments: 1) PID controller; 2) FIM controller and 3) FAIM controller. For each case, comparison experiments are conducted.

Controller parameters are $k_{\rm p} = 0.2,\ k_{\rm i} = 1.0,\ k_{\rm d} = 0.1,\ L = 6,\ \beta = 0.9$ and $T_{\rm s} = 1$ ms respectively. The detail results are given as follows.

1) The parameters $k_{\rm p},\ k_{\rm i}$ and $k_{\rm d}$ of the PID controller are chosen for both stability and performance of the system. Besides, the bandwidth of the system with the PID controller is guaranteed to be about 80 Hz for trajectory tracking.
2) As the key parameter of the FIM and FAIM controllers, L is chosen as a trade-off between tracking performances and practical ease of real-time implementation. With such choice of $L = 6$, during each sampling period ($T_{\rm s} = 1$ ms), $T_{\rm FAIM} \approx 7300$ and $T_{\rm FIM} \approx 80$. In practical experiments, the controllers are implemented via a 375 MHz TMS320C6748 floating-point DSP with up to 2746 million floating-point operations per second (MFLOPS). The DSP can at least perform 80000 multiplication and division operations in 1 ms. So the designed controllers are practically feasible.
3) The parameter β of the feedback filter is chosen as $\beta = 0.9$ mainly for the closed-loop stability of the FIM and FAIM controllers.

At first, an experiment for showing the approximation performance of the proposed FHM is executed. Composed of different frequencies, the input voltage is chosen as $u_v(kT_s) = 1.5\exp(-2.5kT_s)(\sin(120\pi kT_s\exp(-1.2kT_s)) + 1) + 4$. Fig. 5 shows the result of comparing the measured hysteresis curve with the approximated hysteresis curve from FHM. The maximum modelling error is 0.46%. Clearly, the result indicates that the developed FHM can effectively match the hysteresis of piezoelectric actuators.

The input voltage for initial FHM identification is shown as Fig. 6. It should be noted that the voltage is not amplified by the voltage amplifier.

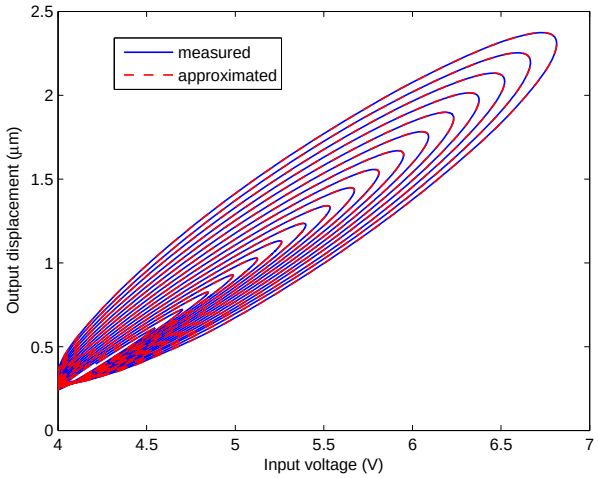

Fig. 5. The measured and approximated hysteresis curve on different input frequencies.

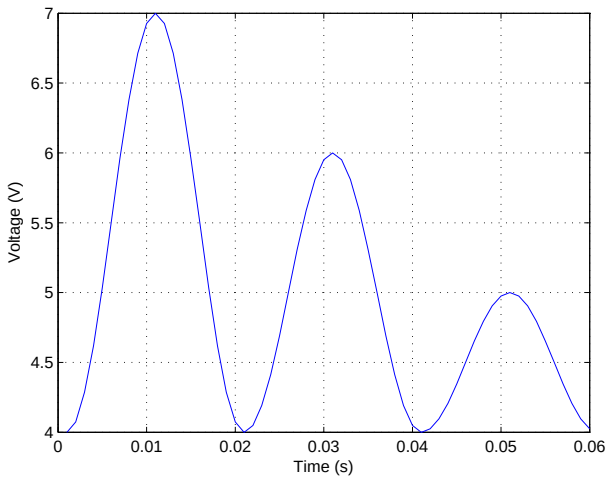

Fig. 6. Input voltage for FHM identification.

A. Single frequency sinusoidal waveform

The desired trajectory is chosen as $y_{\rm d} = 1.0 + 0.8\sin(100\pi t)$ μm, whose frequency is 50 Hz. In Fig. 7 and Fig. 8, tracking results and errors are compared among the PID, FIM and FAIM controllers. As seen, the PID controller can not compensate for the hysteresis effect at the high frequency of 50 Hz, while the FIM controller can achieve about 5 times better tracking performance than the PID controller. The maximum tracking error of the FIM controller is 68.7 nm, which needs to be further reduced by the FAIM controller. Being 92% less than 68.7 nm, the maximum tracking error of the FAIM controller at the last period of $y_{\rm d}$ is 5.8 nm. Fig. 9 shows the results of hysteresis effect compensations of the controllers. The maximum tracking error obtained by the FAIM controller is 0.32%, while that achieved by Ref. [21] was 1.40% for 50 Hz (the same frequency) sinusoidal waveform trajectory. Besides, the maximum tracking error was 3.35% achieved by the model predictive output integral discrete-time sliding mode controller [40] for the 4 Hz trajectory; for lower frequency of 0.01 Hz, the maximum tracking error was 2.50% when the combined cascaded PD/lead-lag feedback controller with the feedforward hysteresis compensator [9] was applied. Clearly the proposed FAIM controller can achieve nanometer-scale precision for high-speed tracking applications.

B. Multiple frequency sinusoidal waveform

Including 25 Hz and 50 Hz frequency, the desired trajectory is $y_{\rm d} = 1.1 + 0.5\sin(100\pi t) + 0.35\sin(50\pi t)$ μm. Figures 10 and 11 show the tracking results and errors of the controllers respectively. From Fig. 11, the maximum tracking error of the FIM controller is 100 nm, while that of the FAIM controller is 29 nm. Illustrated in Fig. 12, the multi-loop rate-dependent

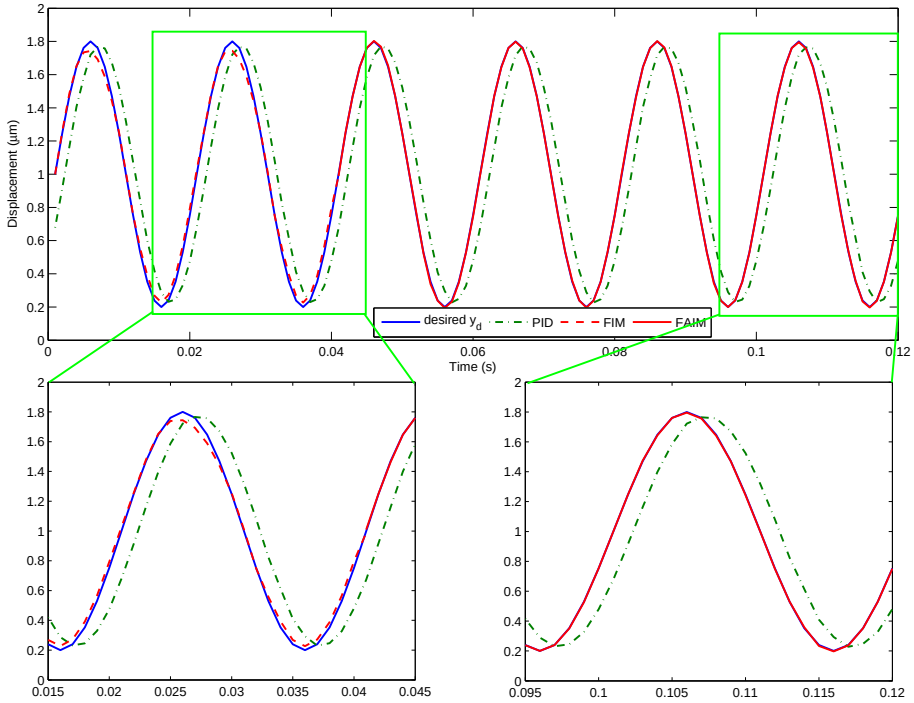

Fig. 7. Tracking results for 50 Hz sinusoidal waveform trajectory.

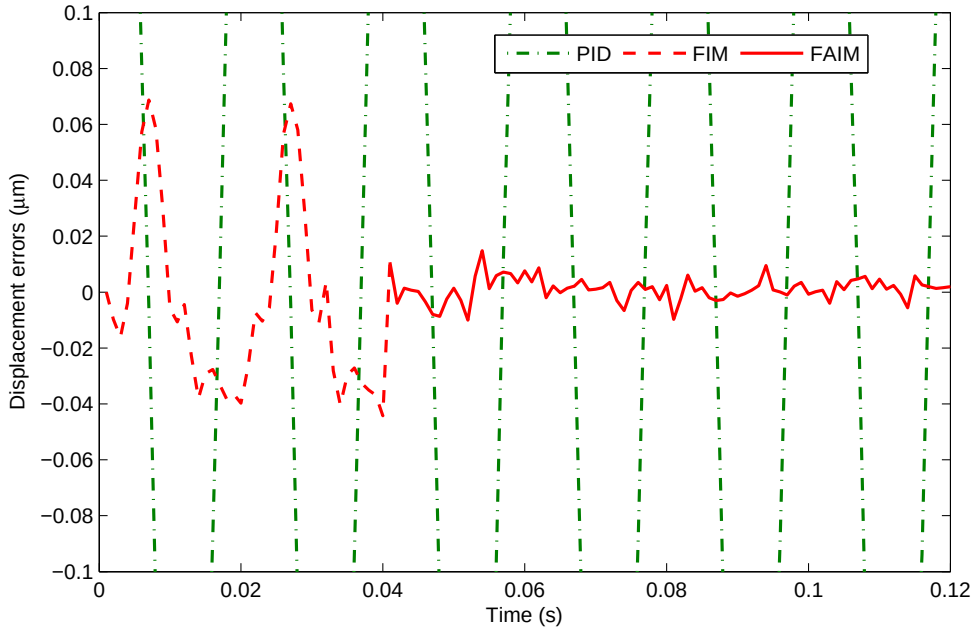

Fig. 8. Tracking errors for 50 Hz sinusoidal waveform trajectory.

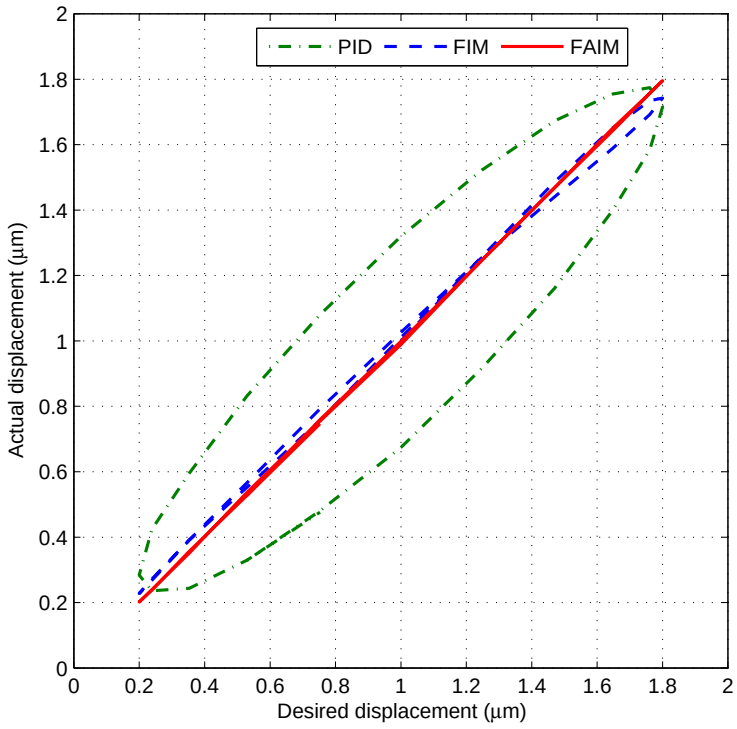

Fig. 9. Results of hysteresis effect compensations for 50 Hz sinusoidal waveform trajectory.

hysteresis effect is greatly decreased by the FAIM controller. In fact, higher performance can be attained by choosing larger L at a slightly higher cost of real-time computational burden. Besides, more periods of $y_{\rm d}$ run, better performance of the FAIM controller achieved.

In summary, tracking performances of the proposed three different controllers (PID, FIM and FAIM) for the two cases of trajectories (50Hz and 50Hz+25Hz) are shown in Table I.

TABLE I
TRACKING PERFORMANCES OF THREE DIFFERENT CONTROLLERS FOR TWO CASES OF TRAJECTORIES.

Desired trajectory (μm)	Controller	$e_{\rm ma}$[a] (nm)	$e_{\rm mr}$[b] (%)	$e_{\rm rms}$[c] (nm)
$y_{\rm d} = 1.0 + 0.8\sin(100\pi t)$	PID	336.0	18.67	231.1
	FIM	68.7	3.82	33.8
	FAIM	5.8	0.32[d]	3.3
$y_{\rm d} = 1.1 + 0.5\sin(100\pi t)$ $+ 0.35\sin(50\pi t)$	PID	290.6	15.64	155.9
	FIM	100.0	5.38	42.4
	FAIM	29.0	1.56	8.5

[a] $e_{\rm ma} = \max\left(|y_{\rm d} - y|\right)$.
[b] $e_{\rm mr} = \max\left(|y_{\rm d} - y|\right) / \max(y_{\rm d})$.
[c] $e_{\rm rms} = \sqrt{\left(\sum (y_{\rm d} - y)^2\right)/N}$.
[d] $e_{\rm mr}$ of other proposed controllers: 1.40% at 50 Hz [21]; 3.35% at 4 Hz [40]; 2.50% at 0.01 Hz [9].

V. CONCLUSIONS

In this paper, an on-line T-S FHM is proposed for hysteresis in piezoelectric actuators. Based on the inverse of the developed FHM, a FIM controller is designed to decrease the hysteresis effect. To achieve nanometer-scale tracking precision, the FAIM controller is uniquely developed. Finally, the experimental results for two cases are shown, the first is with 50 Hz and the other with multiple frequency sinusoidal trajectories tracking that demonstrate the nanometer-scale tracking performance of the novel FAIM controller. Especially, being 0.32% of the maximum desired displacement, the maximum error of 50 Hz sinusoidal tracking is greatly reduced to 6 nm. Nevertheless, further developments of the proposed control strategy will include: 1) more precise identification of FHM; 2) less computational time of FAIM controller and 3) more systematic design and choice of feedback filter for both stability and performance of FAIM controller.

ACKNOWLEDGEMENTS

The authors appreciate the valuable and constructive comments from the anonymous reviewers.

REFERENCES

[1] H. C. Liaw and B. Shirinzadeh, "Robust adaptive constrained motion tracking control of piezo-actuated flexure-based mechanisms for micro/nano manipulation," *IEEE Transactions on Industrial Electronics*, vol. 58, no. 4, pp. 1406 – 1415, Apr. 2011.

[2] C.-M. Lin and H.-Y. Li, "Intelligent control using the wavelet fuzzy CMAC backstepping control system for two-axis linear piezoelectric ceramic motor drive systems," *IEEE Transactions on Fuzzy Systems*, vol. 22, no. 4, pp. 791 – 802, Aug. 2014.

[3] Y. K. Yong, S. O. R. Moheimani, B. J. Kenton, and K. K. Leang, "High-speed flexure-guided nanopositioning: mechanical design and control issues," *Review of Scientific Instruments*, vol. 83, pp. 121 101 – 121 101–22, 2012.

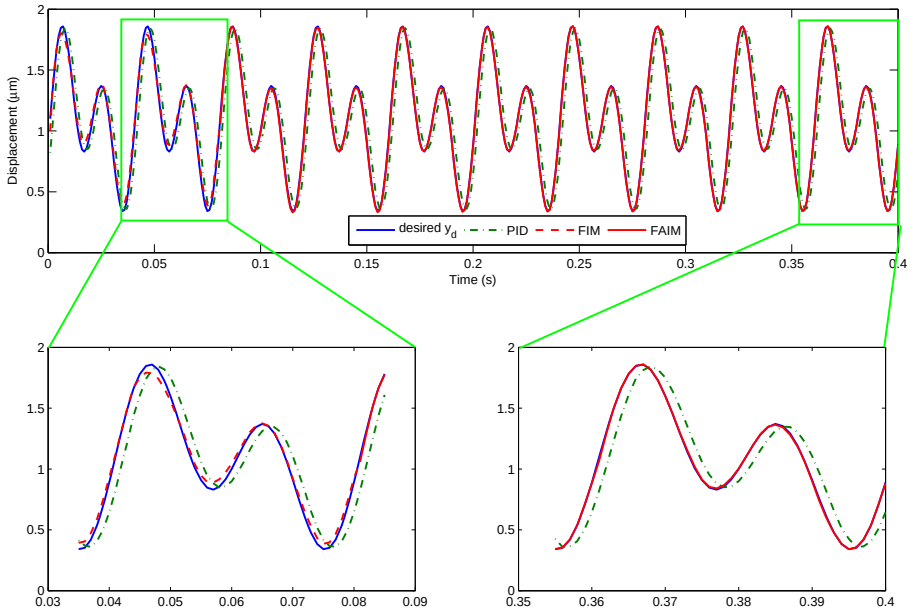

Fig. 10. Tracking results for multiple frequency sinusoidal waveform trajectory.

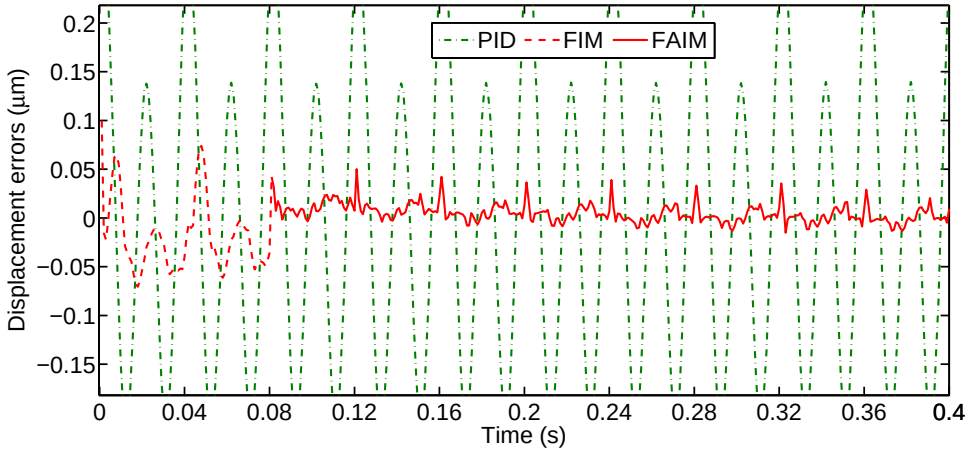

Fig. 11. Tracking errors for multiple frequency sinusoidal waveform trajectory.

[4] L.-J. Lai, G.-Y. Gu, and L.-M. Zhu, "Design and control of a decoupled two degree of freedom translational parallel micro-positioning stage," *Review of Scientific Instruments*, vol. 83, pp. 045 105 – 045 105–17, 2012.

[5] X. L. Dean-Ben and D. Razansky, "Adding fifth dimension to optoacoustic imaging: volumetric time-resolved spectrally enriched tomography," *Light: Science & Applications*, vol. 3, p. e137, 2014.

[6] N. Accanto, J. B. Nieder, L. Piatkowski, M. Castro-Lopez, F. Pastorelli, D. Brinks, and N. F. van Hulst, "Phase control of femtosecond pulses on the nanoscale using second harmonic nanoparticles," *Light: Science & Applications*, vol. 3, p. e143, 2014.

[7] P. Ge and M. Jouaneh, "Tracking control of a piezoceramic actuator," *IEEE Transactions on Control Systems Technology*, vol. 4, no. 3, pp. 209 – 216, May 1996.

[8] I. D. Mayergoyz, "Dynamic Preisach models of hysteresis," *IEEE Transactions on Magnetics*, vol. 24, no. 6, pp. 2925 – 2927, Nov. 1988.

[9] G. Song, J. Zhao, X. Zhou, and J. A. D. Abreu-Garcia, "Tracking control of a piezoceramic actuator with hysteresis compensation using inverse Preisach model," *IEEE/ASME Transactions on Mechatronics*, vol. 10, no. 2, pp. 198 – 209, Apr. 2005.

[10] S. Bobbio, G. Miano, C. Serpico, and C. Visone, "Models of magnetic hysteresis based on play and stop hysterons," *IEEE Transactions on Magnetics*, vol. 33, no. 6, pp. 4417 – 4426, Nov. 1997.

[11] M. Goldfarb and N. Celanovic, "Modeling piezoelectric stack actuators for control of micromanipulation," *IEEE Control Systems Magazine*, vol. 17, no. 3, pp. 69 – 79, Jun. 1997.

[12] L. O. Chua and S. C. Bass, "A generalized hysteresis model," *IEEE Transactions on Circuit Theory*, vol. CT-19, no. 1, pp. 36 – 48, Jan. 1972.

[13] J. Oh and D. S. Bernstein, "Semilinear Duhem model for rate-independent and rate-dependent hysteresis," *IEEE Transactions on Automatic Control*, vol. 50, no. 5, pp. 631 – 645, May 2005.

[14] D. Jiles and J. Thoelke, "Theory of ferromagnetic hysteresis determination of model parameters from experimental hysteresis loops," *IEEE Transactions on Magnetics*, vol. 25, no. 5, pp. 3928 – 3930, Sep. 1989.

[15] L. Deng and Y. Tan, "Diagonal recurrent neural network with modified

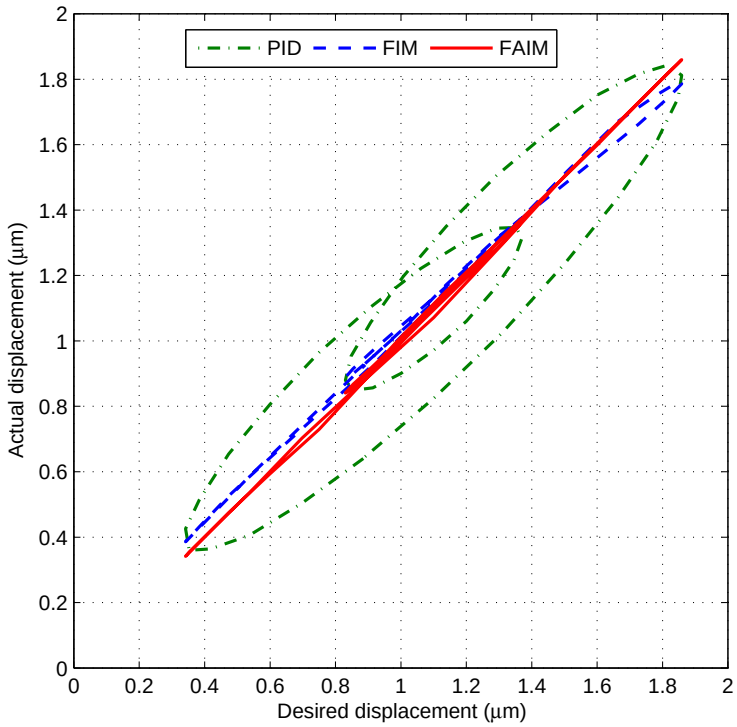

Fig. 12. Results of hysteresis effect compensations for multiple frequency sinusoidal waveform trajectory.

backlash operators for modeling of rate-dependent hysteresis in piezoelectric actuators," *Sensors and Actuators A: Physical*, vol. 148, no. 1, pp. 259 – 270, 2008.

[16] W. T. Ang, P. K. Khosla, and C. N. Riviere, "Feedforward controller with inverse rate-dependent model for piezoelectric actuators in trajectory-tracking applications," *IEEE/ASME Transactions on Mechatronics*, vol. 12, no. 2, pp. 134 –142, Apr. 2007.

[17] M. A. Janaideh, S. Rakheja, and C.-Y. Su, "An analytical generalized PrandtlIshlinskii model inversion for hysteresis compensation in micropositioning control," *IEEE/ASME Transactions on Mechatronics*, vol. 16, no. 4, pp. 734 – 744, Aug. 2011.

[18] Y. Cao and X. B. Chen, "A novel discrete ARMA-based model for piezoelectric actuator hysteresis," *IEEE/ASME Transactions on Mechatronics*, vol. 17, no. 4, pp. 737 – 744, Aug. 2012.

[19] Y. L. Zhang, M. L. Han, M. Y. Yu, C. Y. Shee, and W. T. Ang, "Automatic hysteresis modeling of piezoelectric micromanipulator in vision-guided micromanipulation systems," *IEEE/ASME Transactions on Mechatronics*, vol. 17, no. 3, pp. 547 – 553, Jun. 2012.

[20] S. Tien, Q. Zou, and S. Devasia, "Iterative control of dynamics-coupling-caused errors in piezoscanners during high-speed AFM operation," *IEEE Transactions on Control Systems Technology*, vol. 13, no. 6, pp. 921 – 931, Nov. 2005.

[21] S. Bashash and N. Jalili, "Robust multiple frequency trajectory tracking control of piezoelectrically driven micro/nanopositioning systems," *IEEE Transactions on Control Systems Technology*, vol. 15, no. 5, pp. 867–878, Sep. 2007.

[22] C.-L. Hwang and C. Jan, "Optimal and reinforced robustness designs of fuzzy variable structure tracking control for a piezoelectric actuator system," *IEEE Transactions on Fuzzy Systems*, vol. 11, no. 4, pp. 507 – 517, Aug. 2003.

[23] G. Song, V. Chaudhry, and C. Batur, "Precision tracking control of shape memory alloy actuators using neural networks and a sliding-mode based robust controller," *Smart Material and Structures*, vol. 12, pp. 223–231, 2003.

[24] P.-B. Nguyen and S.-B. Choi, "Compensator design for hysteresis of a stacked PZT actuator using a congruency-based hysteresis model," *Smart Materials and Structures*, vol. 21, pp. 015 009 – 9, 2012.

[25] P.-K. Wong, Q. Xu, C.-M. Vong, and H.-C. Wong, "Rate-dependent hysteresis modeling and control of a piezostage using online support vector machine and relevance vector machine," *IEEE Transactions on Industrial Electronics*, vol. 59, no. 4, pp. 1988 – 2001, Apr. 2012.

[26] W. F. Xie and A. B. Rad, "Fuzzy adaptive internal model control," *IEEE Transactions on Industrial Electronics*, vol. 47, no. 1, pp. 193 – 202, Feb. 2000.

[27] R. Boukezzoula, S. Galichet, and L. Foulloy, "Nonlinear internal model control: application of inverse model based fuzzy control," *IEEE Transactions on Fuzzy Systems*, vol. 11, no. 6, pp. 814 – 829, Dec. 2003.

[28] G. Tsekouras, H. Sarimveis, and G. Bafas, "A simple algorithm for training fuzzy systems using input-output data," *Advances in Engineering Software*, vol. 34, pp. 247 – 259, 2003.

[29] A. Adly and S. Abd-El-Hafiz, "Efficient modeling of vector hysteresis using fuzzy inference systems," *Physica B*, vol. 403, pp. 3812 – 3818, 2008.

[30] P. Li, F. Yan, C. Ge, X. Wang, L. Xu, J. Guo, and P. Li, "A simple fuzzy system for modelling of both rate-independent and rate-dependent hysteresis in piezoelectric actuators," *Mechanical Systems and Signal Processing*, vol. 36, no. 1, pp. 182 – 192, Mar. 2013.

[31] G. Feng, "A survey on analysis and design of model-based fuzzy control systems," *IEEE Transactions on Fuzzy Systems*, vol. 14, no. 5, pp. 676 – 697, 2006.

[32] L.-X. Wang, "Stable adaptive fuzzy control of nonlinear systems," *IEEE Transactions on Fuzzy Systems*, vol. 1, no. 2, pp. 146 – 155, May 1993.

[33] S. Yordanova, D. Merazchiev, and L. Jain, "A two-variable fuzzy control design with application to an air-conditioning system," *IEEE Transactions on Fuzzy Systems*, vol. 23, no. 2, pp. 474 – 481, Apr. 2015.

[34] R. Qi, G. Tao, B. Jiang, and C. Tan, "Adaptive control schemes for discrete-time T-S fuzzy systems with unknown parameters and actuator failures," *IEEE Transactions on Fuzzy Systems*, vol. 20, no. 3, pp. 471 – 486, Jun. 2012.

[35] J. Dong and G.-H. Yang, "Reliable state feedback control of T-S fuzzy systems with sensor faults," *IEEE Transactions on Fuzzy Systems*, vol. 23, no. 2, pp. 421 – 433, Apr. 2015.

[36] T. Takagi and M. Sugeno, "Fuzzy identification of systems and its applications to modeling and control," *IEEE Transactions on Systems, Man and Cybernetics*, vol. SMC-15, no. 1, pp. 116 – 132, Jan. 1985.

[37] Q. Gao, L. Liu, G. Feng, Y. Wang, and J. Qiu, “Universal fuzzy integral sliding-mode controllers based on T-S fuzzy models,” *IEEE Transactions on Fuzzy Systems*, vol. 22, no. 2, pp. 350 – 362, Apr. 2014.

[38] S. G. Devi, K. Selvam, and D. S. P. Rajagopalan, “An abstract to calculate big O factors of time and space complexity of machine code,” in *Chennai and Dr.MGR University Second International Conference on Sustainable Energy and Intelligent System (SEISCON 2011)*. Dr. M.G.R. University, Chennai, India: IET, Jul. 2011, pp. 844 – 847.

[39] K. H. Ang, G. Chong, and Y. Li, “PID control system analysis, design, and technology,” *IEEE Transactions on Control Systems Technology*, vol. 13, no. 4, pp. 559 – 576, Jul. 2005.

[40] Q. Xu and Y. Li, “Micro-/Nanopositioning using model predictive output integral discrete sliding mode control,” *IEEE Transactions on Industrial Electronics*, vol. 59, no. 2, pp. 1161 – 1170, Feb. 2012.